CANADIAN APPLIED
MATHEMATICS QUARTERLY
Volume 8, Number 4, Winter 2000

ON THE FINITE-AMPLITUDE DEVELOPMENT OF NEAR-SINGULAR MODES OF THE BICKLEY JET

GORDON E. SWATERS

ABSTRACT. The linear stability spectrum of the Bickley jet has neutral modes which have a phase velocity equal to the maximum jet velocity. Previous numerical simulations initialized with a monochromatic near-singular mode with a nonzero phase shift across the critical levels have shown that there is a slow time oscillation in the transverse transport of perturbation energy in which the energy flux goes from one critical level to the other and then reverses and so on, all the while satisfying no net energy transfer from the mean flow to the perturbation field. Weakly nonlinear asymptotics suggests that higher harmonics are generated in the critical layer. However, previous numerical simulations do not seem to suggest the development of these modes. Here we examine numerically the evolution of these higher harmonics by initializing a simulation with them explicitly present.

1. Introduction. The *Bickley jet*, [**6, 20**], has been extensively used to model intense currents. Originally derived as an approximate steady jet solution to the Prandtl boundary layer equations [**6**], the Bickley jet has been used to examine the stability of gaseous jets, e.g., [**20**], midlatitude atmospheric jets, e.g., [**15**], oceanic thermocline jets, e.g., [**21**], and the wake behind a bluff body, e.g., [**18**], among many other applications.

Lipps [**15**] found both a neutral sinuous and a varicose normal mode solution to the inviscid linear stability problem for the Bickley jet with the critical levels located at the inflection points. Using Lin's perturbation procedure [**13, 14, 24**], Lipps was able to construct neutral boundaries. Howard and Drazin [**11**] added to the linear stability spectrum by constructing a singular sinuous neutral mode solution to the linear stability problem which had a critical level located at the point of maximum jet velocity. Unlike the perturbation stream function associated with a simple critical level in a homogeneous fluid, the stream function for the Howard and Drazin model is algebraically singular at the critical level. Maslowe [**16**] showed, based on numerical

solutions of the linear stability problem, that the singular neutral mode discovered by Howard and Drazin is part of the lower stability boundary for the varicose mode found by Lipps.

Swaters [**23**] investigated numerically the nonlinear evolution of "near-singular" perturbations (in which the phase velocity of the initial perturbation is asymptotically near but not equal to the maximum jet velocity) to the Bickley jet and showed that these modes are stable over time. However, these simulations also showed that there was a clearly defined "slow time" oscillation in the wave number power spectrum of the perturbation stream function. For an initial near-singular mode with a nonzero phase shift across the critical levels, Swaters showed that there was a slow time oscillation in the transverse transport of perturbation energy in which the energy flux goes from one critical level to the other and then reverses and so on, all the while satisfying no net energy transfer from the mean flow to the perturbation field.

One curious feature of the Swaters' [**23**] simulations was the fact that higher harmonics did not seem to arise in the simulations even though it seems inescapable that weakly nonlinear theory suggests that they must develop. Here we determine the structure of the leading order higher harmonics and use this to "seed" numerical simulations in order to examine the evolution of these terms.

2. Governing equations. The nondimensional, inviscid, incompressible two-dimensional Navier-Stokes equations can be written in the form

$$\Delta\psi_t + J(\psi, \Delta\psi) = 0, \tag{2.1}$$

where the Jacobian is defined by $J(A, B) \equiv A_x B_y - A_y B_x$ where alphabetical subscripts, unless otherwise noted, imply the appropriate partial derivative, and where the stream function $\psi(x, y, t)$ is related to the velocity $\mathbf{u}(x, y, t)$ field via $\mathbf{u} = \mathbf{e}_3 \times \nabla\psi = (-\psi_y, \psi_x)$ and $\Delta = \partial_{xx} + \partial_{yy}$ and t is time.

The Bickley jet stream function, given by

$$\psi = \psi_0(y) = -\tanh(y), \quad -\infty < y < \infty, \tag{2.2}$$

with corresponding velocity field

$$\mathbf{u} = \mathbf{u}_0(y) = (U_0(y), 0) = (\operatorname{sech}^2(y), 0), \tag{2.3}$$

is an exact solution to (2.1).

If we assume a perturbed Bickley jet solution to (2.1) of the form

$$\psi = \psi_0(y) + \{\varphi(y)\exp[ik(x-ct)] + \text{c.c.}\}, \tag{2.4}$$

where k and c are the x-direction wavenumber and complex-valued phase velocity, respectively, where c.c. means complex conjugate and neglect the quadratic perturbation terms, we obtain the Rayleigh stability equation

$$(U_0 - c)(\partial_{yy} - k^2)\varphi - U_{0yy}\varphi = 0, \tag{2.5}$$

which is solved subject to $|\varphi| \to 0$ as $|y| \to \infty$.

Howard and Drazin [**11**] found the singular neutral mode solution for (2.5) given by

$$\varphi = D\frac{\coth(y)}{\cosh^3(y)} \quad \text{for } (c,k) = (1,3), \tag{2.6}$$

where D is a free amplitude constant. At the critical level, located at the jet maximum, given by $y = 0$, φ is algebraically singular and has the Taylor expansion

$$\varphi \simeq D\left\{\frac{1}{y} - \frac{7y}{6} + \frac{307y^3}{360} - \frac{7717y^5}{15120} + O(y^7)\right\}. \tag{2.7}$$

Our goal is to examine the finite-amplitude evolution of a near-singular mode for which

$$k = 3 \quad \text{and} \quad c = 1 - \varepsilon, \quad \text{where } 0 < \varepsilon \ll 1. \tag{2.8}$$

It is instructive to examine the linear asymptotic balances which arise from substituting (2.8) into (2.5). We have

$$\left[\frac{1}{\cosh^2(y)} - 1 + \varepsilon\right](\partial_{yy} - 9)\varphi + \left[\frac{2}{\cosh^4(y)} - \frac{4\tanh^2(y)}{\cosh^2(y)}\right]\varphi = 0. \tag{2.9}$$

Assuming a straightforward asymptotic solution to (2.9) of the form

$$\varphi \simeq \varphi^{(0)} + \varepsilon\varphi^{(1)} + \cdots,$$

leads to the leading order problem given by

$$\left[\frac{1}{\cosh^2(y)}-1\right](\partial_{yy}-9)\varphi^{(0)}+\left[\frac{2}{\cosh^4(y)}-\frac{4\tanh^2(y)}{\cosh^2(y)}\right]\varphi^{(0)}=0. \tag{2.10}$$

The solution for $\varphi^{(0)}$ we are interested in is given by (2.6).

However, there is clearly a distinguished limit in (2.9) for $y \simeq O(\sqrt{\varepsilon})$. Introducing the variable χ, defined by $y = \sqrt{\varepsilon}\chi$ and $\varphi = \tilde{\varphi}(\chi)$ into (2.9) leads to

$$\left[(1-\chi^2)+\frac{2\varepsilon}{3}\chi^4\right](\partial_{\chi\chi}-9\varepsilon)\tilde{\varphi}+(2-8\varepsilon\chi^2)\tilde{\varphi}+O(\varepsilon^2)=0. \tag{2.11}$$

If we assume a straightforward asymptotic solution to (2.11) of the form

$$\bar{\varphi} \simeq \bar{\varphi}^{(0)} + \varepsilon\tilde{\varphi}^{(1)} + \cdots, \tag{2.12}$$

the $O(1)$ problem is given by

$$(1-\chi^2)\tilde{\varphi}^{(0)}_{\chi\chi} + 2\tilde{\varphi}^{(0)} = 0, \tag{2.13}$$

which has the general solution

$$\tilde{\varphi}^{(0)} = B(1-\chi^2) + A\left[\chi + \frac{1}{2}(1-\chi^2)\ln\left(\frac{\chi+1}{\chi-1}\right)\right], \tag{2.14}$$

where B and A are arbitrary constants.

The solution for $\tilde{\varphi}^{(0)}$ has two branch points located at $\chi = \pm 1$, which correspond to the asymptotically displaced critical levels written in terms of the variable χ. The essential issue is to determine the appropriate relations connecting A and B in the regions $|\chi| > 1$ and $|\chi| < 1$, respectively.

We may assume that the argument of the logarithmic term in $\tilde{\varphi}^{(0)}$ is determined by its absolute value and determine B accordingly. This is equivalent to introducing the appropriate branch cut for the logarithmic function when viewed as a complex valued function or, equivalently, the requisite phase shift, if any, across the critical levels.

We can immediately see that $B = 0$ in the regions $|\chi| > 1$ since $\tilde{\varphi}^{(0)}$ must asymptotically match with $\varphi^{(0)}$ as $|\chi| \to \infty$ and $y \to 0$, respectively, and $\varphi^{(0)}$ and the second term in (2.14) are both odd functions, but the first term in (2.14), which is proportional to $1 - \chi^2$, is even.

The $|\chi| \gg 1$ structure of $\tilde{\varphi}^{(0)}$ is therefore given by

$$\tilde{\varphi}^{(0)} \simeq 2A\left\{\frac{1}{3\chi} + \frac{1}{15\chi^3} + \frac{1}{35\chi^5} + \frac{1}{63\chi^7} + O(\chi^{-9})\right\}, \tag{2.15}$$

or, in terms of y,

$$\tilde{\varphi}^{(0)} \simeq 2A\sqrt{\varepsilon}\left\{\frac{1}{3y} + \frac{\varepsilon}{15y^3} + \frac{\varepsilon^2}{35y^5} + \frac{\varepsilon^3}{63y^7} + O(\varepsilon^4)\right\}. \tag{2.16}$$

Comparing (2.7) and (2.16) leads to the relation

$$D = \frac{2\sqrt{\varepsilon}}{3}A, \tag{2.17}$$

for the regions $|\chi| > 1$.

To complete the determination of A and B requires examining higher order problems in the asymptotic expansion (including the appropriate slow space and time derivatives). However, as is well known, e.g., [**3, 5, 17**], the individual solutions become progressively disordered, i.e., increasingly singular, at the critical levels $\chi = \pm 1$. The spatial regularization of the stream function across the critical levels can be achieved by examining sub layers centered at $\chi = \pm 1$, respectively, in which physics are not included in the Rayleigh stability equation, e.g., time dependence, friction or nonlinearity, cannot be neglected, see, e.g., [**4, 7, 8, 25**].

Because the asymptotically displaced critical levels, located at $\chi = \pm 1$, are simple, classical linear viscous critical layer theory, see, e.g., [**9, 25**] would imply that

$$B = \frac{i\pi A}{2} \quad \text{for } |\chi| < 1. \tag{2.18}$$

On the other hand, if nonlinearity dominates in the critical layer, then it is known, see, e.g., [**4, 9, 10**], that

$$B = 0 \quad \text{for } |\chi| < 1. \tag{2.19}$$

Indeed, as shown by Haberman [**10**], see also the discussion in [Sections 27 and 52.5, **9**], the value of B is a monotonic function of the dimensionless parameter $\lambda = (\alpha^{3/2} R_e)^{-1}$, where α is the dimensionless amplitude of the normal mode perturbation. In particular, $B \to 0$ as $\lambda \to 0$, i.e., nonlinearity dominates, and $B \to i\pi A/2$ as $\lambda \to \infty$, i.e., linear viscous dynamics dominates.

If we assume that, to leading order, the transverse structure of the *initial* perturbation stream function in the region $y \simeq O(\sqrt{\varepsilon})$ is described by (2.13), this implies that, at least initially, we are assuming that the nonlinear terms are small. This, in turn, puts a constraint on our choice of the magnitude of the initial amplitude of the perturbation. If one examines the asymptotic balances which arise by assuming $y \simeq O(\sqrt{\varepsilon})$, $(x,t) \simeq O(1)$, since $(k,c) \simeq O(1)$ for $(c,k) = (1-\varepsilon, \pm 3)$, and $\varphi \simeq O(A)$, it follows that we must choose $A \simeq O(\varepsilon^2)$ at most in order that the nonlinear terms will not appear in the leading order linear balance, which we insist must be given by (2.13), at least initially. As it turns out, the choice $A \simeq O(\varepsilon^{5/2})$ will imply that the nonlinear terms in the $y \simeq O(\sqrt{\varepsilon})$ region will be $O(\varepsilon)$ compared to the leading order balance.

Thus, the finite-amplitude evolution of near-singular modes of the Bickley jet requires examining outer, intermediate and inner regions. In the outer region, where the perturbation stream function is exponentially small, the dynamics is essentially linear. In this region the critical levels appear to have coalesced producing an algebraically singular structure in the stream function at the point of maximum jet velocity.

The intermediate region, described by the variable χ, is also weakly nonlinear and separates the algebraic singularity located at the jet maximum into two symmetrically placed simple critical levels. The inner regions, which do not concern us here, will complete the determination of the spatial regularization.

3. Weakly nonlinear dynamics. It is convenient to introduce the fast phase and slow space-time variables, given by, respectively,

$$\theta = x - (1-\varepsilon)t, \quad (X,T) = \varepsilon^2(x,t), \quad \tau = \varepsilon^3 t. \tag{3.1}$$

Substitution of (3.1) into (2.1) leads to

$$
\begin{aligned}
(3.2)\quad & [(\varepsilon-1)\partial_\theta+\varepsilon^2\partial_T+\varepsilon^3\partial_\tau][\Delta+2\varepsilon^2\partial_{\theta X}+\varepsilon^4\partial_{XX}]\psi \\
& \quad +(\psi_\theta+\varepsilon^2\psi_X)[\Delta\psi_y+2\varepsilon^2\psi_{y\theta X}+\varepsilon^4\psi_{yXX}] \\
& \quad -\psi_y(\partial_\theta+\varepsilon^2\partial_X)[\Delta\psi+2\varepsilon^2\psi_{\theta X}+\varepsilon^4\psi_{XX}]=0,
\end{aligned}
$$

where $\Delta=\partial_{\theta\theta}+\partial_{yy}$.

In the outer regions, where $|y|\gtrsim O(1)$, we may write the solution to (3.2) in the form

$$
(3.3)\qquad \psi(\theta,y,X,T,\tau)=-\tanh(y)+\varepsilon^3\varphi(\theta,y,X,T,\tau).
$$

Substitution of (3.3) into (3.2) leads to

$$
\begin{aligned}
(3.4)\quad & [(U_0-1+\varepsilon)\partial_\theta+\varepsilon^2(\partial_T+U_0\partial_X)+\varepsilon^3\partial_\tau][\Delta+2\varepsilon^2\partial_{\theta X}+\varepsilon^4\partial_{XX}]\varphi \\
& -U_{0yy}(\partial_\theta+\varepsilon^2\partial_X)\varphi+\varepsilon^3\big\{(\varphi_\theta+\varepsilon^2\varphi_X)[\Delta\varphi_y+2\varepsilon^2\varphi_{y\theta X}+\varepsilon^4\varphi_{yXX}] \\
& \quad -\varphi_y(\partial_\theta+\varepsilon^2\partial_X)[\Delta\varphi+2\varepsilon^2\varphi_{\theta X}+\varepsilon^4\varphi_{XX}]\big\}=0,
\end{aligned}
$$

where

$$
(3.5)\qquad U_0(y)=\frac{1}{\cosh^2(y)},\quad U_{0yy}(y)=\frac{4\tanh^2(y)}{\cosh^2(y)}-\frac{2}{\cosh^4(y)}.
$$

The solution to (3.4) can be constructed via the straightforward asymptotic expansion

$$
(3.6)\quad \varphi(\theta,y,X,T,\tau;\varepsilon)\simeq[\varphi^{(0)}+\varepsilon\varphi^{(1)}+\varepsilon^2\varphi^{(2)}](\theta,y,X,T,\tau)+O(\varepsilon^3),
$$

with the $O(1), O(\varepsilon)$ and $O(\varepsilon^2)$ problems given by, respectively,

$$
(3.7)\qquad \mathcal{L}\varphi^{(0)}=0,
$$

$$
(3.8)\qquad \mathcal{L}\varphi^{(1)}=-\Delta\varphi^{(0)}_\theta,
$$

$$
\begin{aligned}
(3.9)\quad \mathcal{L}\varphi^{(2)} &= -\Delta\varphi^{(1)}_\theta-[(\partial_T+U_0\partial_X)\Delta \\
&\quad +2(U_0-1)\partial_{\theta\theta X}-U_{0yy}\partial_X]\varphi^{(0)},
\end{aligned}
$$

and where the linear operator $\mathcal{L}$ is given by

$$
(3.10)\qquad \mathcal{L}=(U_0-1)\Delta\partial_\theta-U_{0yy}\partial_\theta,
$$

and where $U_0(y)$ and $U_{0yy}(y)$ are given by (3.5).

On account of (2.17), it is convenient to write the solution to (3.7) in the form

$$\varphi^{(0)} = \frac{2A(X,T,\tau)\coth(y)}{3\cosh^3(y)}\exp[3i\theta] + \text{c.c.}, \tag{3.11}$$

where it is now assumed that $A(X,T,\tau) \simeq O(1)$.

Substitution of (3.11) into the $O(\varepsilon)$ problem (3.8) leads to

$$\mathcal{R}\varphi_1 = -\frac{U_{0yy}\coth(y)}{(U_0-1)\cosh^3(y)} = \frac{4\coth(y)}{\cosh^5(y)} - \frac{2\coth^3(y)}{\cosh^7(y)}, \tag{3.12}$$

where we have assumed

$$\varphi^{(1)}(\theta,y,X,T,\tau) = \frac{2A(X,T,\tau)}{3}\varphi_1(y)\exp[3i\theta] + \text{c.c.}, \tag{3.13}$$

and where $\mathcal{R}$ is the Rayleigh operator for the $\exp[\pm 3i\theta]$ mode given by

$$\mathcal{R} = (U_0-1)(\partial_{yy}-9) - U_{0yy}. \tag{3.14}$$

The solution to (3.12) is given by

$$\begin{aligned}\varphi_1(y) = {} & \frac{12[\ln(\sinh|y|)-|y|]}{5\sinh(y)\cosh^2(y)} + \frac{1}{5\sinh^3(y)\cosh^2(y)} \\ & - \frac{8\sinh(y)}{5\cosh^2(y)} + \frac{16}{5\sinh(y)} - \frac{12\,\text{sgn}\,(y)}{5\cosh(y)} \\ & + \frac{8}{5}[\text{sgn}\,(y)\cosh(3y) - \sinh(3y)] \\ & + \frac{16}{5}[\text{sgn}\,(y)\cosh(y) - \sinh(y)],\end{aligned} \tag{3.15}$$

where $\text{sgn}\,(y)$ is the sign of y.

Comparing the $O(1)$ and $O(\varepsilon)$ solutions we see that

$$\frac{\varphi^{(1)}}{\varphi^{(0)}} \simeq O(y^{-2}) \quad \text{as } y \to 0. \tag{3.16}$$

Hence we conclude that this expansion becomes spatially nonuniform for $y \simeq O(\sqrt{\varepsilon})$ which was already observed in (2.9).

The $O(\varepsilon^2)$ outer problem given by (3.9) may be rewritten in the form

$$\begin{aligned}\mathcal{R}\varphi_2 = {} & \frac{2AU_{0yy}\varphi_0}{3(U_0-1)^2} - \frac{2AU_{0yy}\varphi_1}{3(U_0-1)} \\ & + \frac{2i\varphi_0}{9}\left\{\frac{U_{0yy}}{U_0-1}\partial_T + \left[\frac{U_{0yy}}{U_0-1} - 18(U_0-1)\right]\partial_X\right\}A,\end{aligned} \tag{3.17}$$

where we have assumed that

$$\varphi^{(2)} = \varphi_2(y, X, T, \tau)\exp(3i\theta) + \text{c.c.} \tag{3.18}$$

All we need are the first few terms of φ_2 as $y \to 0$. Expanding the coefficients of the Rayleigh operator $\mathcal{R}$ and the righthand side of (3.17) yields

$$\begin{aligned}&\left[\left(-y^2 + \frac{2}{3}y^4 - \frac{17}{45}y^6 + \cdots\right)\partial_{yy} + 2 + y^2 + \frac{16}{3}y^4 + \cdots\right]\varphi_2 \\ &= \left[\left(-\frac{8}{5}y^{-5} + \frac{32}{15}y^3 + \frac{29}{3}y^{-1} - \frac{55163}{4725}y\right)\right. \\ &\quad + \left(-\frac{16}{5}y^{-3} + \frac{72}{5}y^{-1} - \frac{1874}{75}y\right)\ln|y| \\ &\quad \left. + \operatorname{sgn}(y)\left(-\frac{256}{15} + \frac{3968}{75}y^2\right)\right]A \\ &\quad + i\left[\left(\frac{4}{9}y^{-3} - 2y^{-1}\right)(A_T + A_X) + \frac{937}{270}yA_T + \frac{2017}{270}yA_X\right] + O(y^3).\end{aligned} \tag{3.19}$$

Correct to $O(1)$ in the variable y, (3.19) has the solution

$$\begin{aligned}\varphi_2 = {} & \frac{2A}{35y^5} + \frac{[(49A/375) - (2i/45)(A_T + A_X)]}{y^3} + \frac{8A}{25}\frac{\ln|y|}{y^3} \\ & + \left[\frac{4132A}{875} - \frac{8i}{15}(A_T + A_X)\right]\frac{\ln|y|}{y} \\ & + \frac{48A}{25}\frac{\ln^2|y|}{y} + O(1).\end{aligned} \tag{3.20}$$

Thus, as $y \to 0$ and to $O(\varepsilon^2)$, it follows that the complete outer solution $\varphi(\theta, y, X, T, \tau)$ has the asymptotic form

(3.21)
$$\begin{aligned}
&\varphi(\theta, y, X, T, \tau; \varepsilon) \simeq \varphi^{(0)} + \varepsilon\varphi^{(1)} + \varepsilon^2\varphi^{(2)} + \cdots \\
&\quad \simeq A(X, T, \tau) \exp[3i\theta] \Bigg\{ \left[\frac{2}{3y} - \frac{7}{9}y + \frac{307}{540}y^3 - \frac{7717}{22680}y^5 + O(y^7) \right] \\
&\qquad + \varepsilon \Bigg[\operatorname{sgn}(y) \left(\frac{128}{15}y^2 + \frac{448}{225}y^4 + \frac{9616}{4725}y^6 \right) \\
&\qquad + \ln|y| \left(\frac{8}{5y} - \frac{28}{15}y + \frac{307}{225}y^3 - \frac{7717}{9450}y^5 \right) \\
&\qquad + \frac{2}{15y^3} + \frac{29}{15y} - \frac{1843}{900}y - \frac{89627}{22680}y^3 \\
&\qquad - \frac{1200377}{504000}y^5 + O(y^7) \Bigg] \\
&\qquad + \varepsilon^2 \left[\frac{2}{35y^5} + \left[\frac{49}{375} - \frac{2i(A_T + A_X)}{45A} \right] \frac{1}{y^3} + \frac{8\ln|y|}{25y^3} \right. \\
&\qquad \left. + \left[\frac{4132}{875} - \frac{8i(A_T + A_X)}{15A} \right] \frac{\ln|y|}{y} + \frac{48\ln^2|y|}{25y} \right] + O(1) \Bigg\} + \text{c.c.}
\end{aligned}$$

It is convenient to write this expression in terms of the variable χ, defined by $y = \sqrt{\varepsilon}\chi$, yielding

(3.22)
$$\begin{aligned}
\varphi \simeq \frac{A(X, T, \tau)}{\sqrt{\varepsilon}} \exp[3i\theta] &\Bigg\{ \frac{2}{3\chi} + \frac{2}{15\chi^3} + \frac{2}{35\chi^5} + \varepsilon\ln(\varepsilon) \left[\frac{4}{25\chi^3} + \frac{4}{5\chi} \right] \\
&+ \varepsilon \Bigg(\left[\frac{49}{375} - \frac{2i(A_T + A_X)}{45A} \right] \frac{1}{\chi^3} + \frac{29}{15\chi} - \frac{7\chi}{9} + \left[\frac{8}{25\chi^3} + \frac{8}{5\chi} \right] \ln|\chi| \Bigg) \\
&+ \frac{12\varepsilon^2\ln^2(\varepsilon)}{25\chi} + \varepsilon^2\ln(\varepsilon) \Bigg(\left[\frac{2066}{875} - \frac{4i(A_T + A_X)}{15A} \right] \frac{1}{\chi} \\
&- \frac{14\chi}{15} + \frac{48\ln|\chi|}{25\chi} \Bigg) + \varepsilon^2 \Bigg(\frac{307\chi^3}{540} - \frac{1843\chi}{900} - \frac{28\chi}{15}\ln|\chi| \\
&+ \left[\frac{4132}{875} - \frac{8i(A_T + A_X)}{15A} \right] \frac{\ln|\chi}{\chi} + \frac{48\ln^2|\chi|}{25\chi} \Bigg) \Bigg\} + \text{c.c.} + O(\varepsilon^3),
\end{aligned}$$

as $\varepsilon \to 0$.

We now turn to determining the structure of the perturbation stream function in the region where $y \simeq O(\sqrt{\varepsilon})$. In this region the critical level which appeared to be located at the jet maximum located $y = 0$ from the point of view of the outer region, has bifurcated into two symmetrically placed critical levels, located at $y = \pm\sqrt{\varepsilon}$ or, in terms of the intermediate variable, $\chi \equiv y/\sqrt{\varepsilon}$, $\chi = \pm 1$.

Another point to observe is that in the intermediate region, as in the outer region, there is a scale separation between the mean flow and the perturbation field. In the intermediate region, as shown below, the perturbation stream function is $O(\varepsilon^{5/2})$ whereas the mean flow stream function which is $O(\sqrt{\varepsilon})$ in this region. It will follow that the dynamics of the intermediate region will be weakly nonlinear as well.

However, in contrast to the outer region where the dynamics was purely linear to the order required in the present analysis, in the intermediate region nonlinear effects begin to appear in the second order problem and in the asymptotic expansion and the production of higher order harmonics, and a secondary mean flow cannot be neglected.

In the intermediate region, where $y \simeq O(\sqrt{\varepsilon})$, we may write the solution to (3.2) in the form

$$\psi(\theta, \chi, X, T, \tau) = -\tanh(\sqrt{\varepsilon}\chi) + \varepsilon^{5/2}\tilde{\varphi}(\theta, \chi, X, T, \tau), \tag{3.23}$$

where, of course, $y = \sqrt{\varepsilon}\chi$. Substitution of (3.23) into (3.2) leads to,

after neglecting terms $O(\varepsilon^3)$ and dropping the tilde for convenience,

(3.24)
$$
\begin{aligned}
[(1-\chi^2)\partial_{\chi\chi}+2]\varphi_\theta +\varepsilon\Bigg\{&\left[\frac{2\chi^4}{3}\partial_{\chi\chi\theta}+(\partial_T+\partial_X)\partial_{\chi\chi}\right.\\
&\left.+(1-\chi^2)\partial_{\theta\theta\theta}-8\chi^2\partial_\theta\right]\varphi+\varphi_\theta\varphi_{\chi\chi\chi}-\varphi_\chi\varphi_{\chi\chi\theta}\Bigg\}\\
+\varepsilon^2\Bigg\{&\left[\partial_{\chi\chi\tau}-\frac{17\chi^6}{45}\partial_{\chi\chi\theta}-\chi^2\partial_{\chi\chi X}+\frac{34\chi^4}{3}\partial_\theta+2\partial_X\right.\\
&\left.+\left(\frac{2\chi^4}{3}\partial_\theta+\partial_T+\partial_X\right)\partial_{\theta\theta}\right]\varphi+\varphi_\theta\varphi_{\chi\theta\theta}-\varphi_\chi\varphi_{\theta\theta\theta}\Bigg\}\\
+O(\varepsilon^3)=0.&
\end{aligned}
$$

Examination of the intermediate region expansion of the outer solution given by (3.22) suggests that we construct an asymptotic solution to (3.24) in the form

$$
\begin{aligned}
\varphi \simeq{}& \varphi^{(0)}+\varepsilon\varphi^{(1,0)}+\varepsilon\ln\varepsilon\varphi^{(1,1)}+\varepsilon^2\ln^2\varepsilon\varphi^{(2,0)}\\
&+\varepsilon^2\ln\varepsilon\varphi^{(2,1)}+O(\varepsilon^2),
\end{aligned}
\tag{3.25}
$$

which results in the $O(1), O(\varepsilon), O(\varepsilon\ln\varepsilon), O(\varepsilon^2\ln\varepsilon)$ and $O(\varepsilon^2\ln^2\varepsilon)$ problems given, respectively, by

$$
[(1-\chi^2)\partial_{\chi\chi}+2]\varphi^{(0)}=0, \tag{3.26}
$$

$$
\begin{aligned}
[(1-\chi^2)\partial_{\chi\chi}+2]\varphi_\theta^{(1,0)} ={}& \varphi_\chi^{(0)}\varphi_{\chi\chi\theta}^{(0)}-\varphi_\theta^{(0)}\varphi_{\chi\chi\chi}^{(0)}\\
&-\left[\frac{2\chi^4}{3}\partial_{\chi\chi\theta}+(\partial_T+\partial_X)\partial_{\chi\chi}+(1-\chi^2)\partial_{\theta\theta\theta}-8\chi^2\partial_\theta\right]\varphi^{(0)},
\end{aligned}
\tag{3.27}
$$

$$
[(1-\chi^2)\partial_{\chi\chi}+2]\varphi_\theta^{(1,1)}=0, \tag{3.28}
$$

$$
[(1-\chi^2)\partial_{\chi\chi}+2]\varphi_\theta^{(2,0)}=0, \tag{3.29}
$$

$$[(1-\chi^2)\partial_{\chi\chi}+2]\varphi_\theta^{(2,1)} = -\left[\frac{2\chi^4}{3}\partial_{\chi\chi\theta}+(\partial_T+\partial_X)\partial_{\chi\chi}+(1-\chi^2)\partial_{\theta\theta\theta}-8\chi^2\partial_\theta\right]\varphi^{(1,1)}. \tag{3.30}$$

The solution to the $O(1)$ problem (3.26) associated with the $3i\theta$-mode may be written in the form

$$\varphi^{(0)}(\theta,\chi,X,T,\tau) = A\Phi(\chi)\exp(3i\theta)+\text{c.c.}, \tag{3.31}$$

with

$$\Phi(\chi) = \chi+\frac{1}{2}(1-\chi^2)\ln\left(\frac{\chi+1}{\chi-1}\right), \tag{3.32}$$

where

$$\ln\left(\frac{\chi+1}{\chi-1}\right) = \begin{cases}\ln|\chi+1/\chi-1| & \text{for } |\chi|>1,\\ \ln|\chi+1/\chi-1|+\delta\pi i & \text{for } |\chi|<1,\end{cases} \tag{3.33}$$

where δ ranges from 0 (the nonlinear critical layer) to 1 (the viscous critical layer).

As $|\chi|\to\infty$, this solution matches the $y\to 0$ structure of the leading order outer solution (3.11). It is important to remember that all our asymptotic matching actually occurs with $\sqrt{\varepsilon}\times$ (3.22) due to the differing amplitude scaling associated with the perturbation stream function in the outer and intermediate expansions (3.3) and (3.23), respectively.

Examination of the $\varepsilon\ln\varepsilon$ and $\varepsilon^2\ln^2\varepsilon$ terms in the intermediate expansion of the outer solution given by (3.22) implies that the only homogeneous solutions to the $O(\varepsilon\ln\varepsilon)$ and $O(\varepsilon^2\ln^2\varepsilon)$ problems (3.28) and (3.29), respectively, which are relevant are those proportional to $\Phi(\chi)$ and are given by, respectively,

$$\varphi^{(1,1)}(\theta,\chi,X,T,\tau) = \frac{6A(X,T,\tau)}{5}\Phi(\chi)\exp(3i\theta)+\text{c.c.}, \tag{3.34}$$

$$\varphi^{(2,0)}(\theta,\chi,X,T,\tau) = \frac{18A(X,T,\tau)}{25}\Phi(\chi)\exp(3i\theta)+\text{c.c.} \tag{3.35}$$

Note that, as required, the first two terms of the large $|\chi|$ expansion of $\varphi^{(1,1)}$ will match to both $O(\varepsilon \ln \varepsilon)$ terms in (3.22) and that the leading order term associated with the large $|\chi|$ expansion of $\varphi^{(2,0)}$ will match to the single $O(\varepsilon^2 \ln^2 \varepsilon)$ term in (3.22).

The $O(\varepsilon)$ problem can be written in the form, after a little algebra,

(3.36)
$$[(1-\chi^2)\partial_{\chi\chi}+2]\varphi_\theta^{(1,0)} = \frac{12i\chi\Phi^2}{(1-\chi^2)^2}A^2\exp(6i\theta) + \left[iA\Phi\left(\frac{4\chi^4}{1-\chi^2}+27-3\chi^2\right) - (A_T+A_X)\Phi_{\chi\chi}\right]\exp(3i\theta)+\text{c.c.}$$

It is convenient to write the particular solution, denoted as $\varphi_p^{(1)}$, in the form

(3.37)
$$\varphi_p^{(1)} = 2A^2F_1(\chi)\exp(6i\theta) + \frac{1}{3}[AF_2(\chi)+i(A_T+A_X)F_3(\chi)]\exp(3i\theta)+\text{c.c.},$$

where $F_1(\chi), F_2(\chi)$ and $F_3(\chi)$ satisfy, respectively, the ordinary differential equations

(3.38)
$$[(1-\chi^2)\partial_{\chi\chi}+2]F_1 = \frac{\chi\Phi^2}{(1-\chi^2)^2},$$

(3.39)
$$[(1-\chi^2)\partial_{\chi\chi}+2]F_2 = \left(\frac{4\chi^4}{1-\chi^2}+27-3\chi^2\right)\Phi,$$

(3.40)
$$[(1-\chi^2)\partial_{\chi\chi}+2]F_3 = \Phi_{\chi\chi}.$$

The solutions for $F_1(\chi), F_2(\chi)$ and F_3 are given by, respectively[1],

(3.41)
$$F_1(\chi) = \frac{\chi}{8(1-\chi^2)} - \frac{1}{2}\ln\left(\frac{\chi+1}{\chi-1}\right) + \frac{\chi}{8}\ln^2\left(\frac{\chi+1}{\chi-1}\right),$$

(3.42)
$$\begin{aligned} F_2(\chi) = {} & \frac{48\chi}{5} + \frac{7\chi^3}{10} + \frac{\chi^2(27-7\chi^2)}{20}\ln\left(\frac{\chi+1}{\chi-1}\right) \\ & + \frac{18}{5}[(1+\chi)\ln(\chi+1) + (\chi-1)\ln(\chi-1)] \\ & + \frac{18}{5}(1-\chi^2)\int_{\text{sign}\,(\chi)\infty}^{\chi}\left[\frac{\ln(\eta-1)}{\eta+1} + \frac{\ln(\eta-1)}{1-\eta}\right]d\eta, \end{aligned}$$

(3.43)
$$F_3(\chi) = -\frac{1}{2}\ln\left(\frac{\chi+1}{\chi-1}\right).$$

The large $|\chi|$ behavior of the term proportional to $\exp(\pm 3i\theta)$ in $\varphi_p^{(1)}$ must match with the $O(\varepsilon)$ term in (3.22). We find that

(3.44)
$$\begin{aligned} & \frac{1}{3}[AF_2(\chi) + i(A_T + A_X)F_3(\chi)] \\ & \quad \simeq A\left[-\frac{7\chi}{9} + \frac{133}{25\chi} + \frac{101}{125\chi^3} + \cdots + \left(\frac{8}{5\chi} + \frac{8}{25\chi^3} + \cdots\right)\ln|\chi|\right] \\ & \qquad - \frac{i(A_T + A_X)}{3}\left[\frac{1}{\chi} + \frac{1}{3\chi^3} + \cdots\right], \end{aligned}$$

as $|\chi| \to \infty$. This will match with the $O(\varepsilon)$ term in (3.22) if and only if

$$\frac{133A}{25} - \frac{i(A_T + A_X)}{3} = \frac{29A}{15},$$

and

$$\frac{101A}{125} - \frac{i(A_T + A_X)}{9} = \frac{49A}{375} - \frac{2i(A_T + A_X)}{45},$$

which arise from matching the $O(\chi^{-1})$ and $O(\chi^{-3})$ terms, respectively.

Both of these expressions can be rearranged into the same form

$$A_T + A_X = -\frac{254i}{25}A, \tag{3.45}$$

which has the general solution

$$A = \tilde{A}(\xi,\tau)\exp\left(-\frac{254i}{25}T\right) \quad \text{with } \xi \equiv X - T. \tag{3.46}$$

The complete solution for $\varphi^{(1,0)}$ can therefore be written in the form

$$\begin{aligned}\varphi^{(1,0)} &= 2A^2F_1(\chi)\exp(6i\theta)\\ &\quad + \frac{A}{3}\left[F_2(\chi) + \frac{254}{25}F_3(\chi)\right]\exp(3i\theta) + \text{c.c.}\end{aligned} \tag{3.47}$$

With the $O(\varepsilon)$ solution complete, solving the $O(\varepsilon^2\ln\varepsilon)$ is straightforward. Substituting (3.34) into (3.30) leads to

$$\begin{aligned}[(1-\chi^2)\partial_{\chi\chi} + 2]\varphi_\theta^{(2,1)} &= -\frac{6}{5}(A_T + A_X)\Phi_{\chi\chi}\exp(3i\theta)\\ &\quad + \frac{6i}{5}\left(\frac{4\chi^4}{1-\chi^2} + 27 - 3\chi^2\right)A\Phi\exp(3i\theta)\\ &\quad + \text{c.c.},\end{aligned} \tag{3.48}$$

where we have written the problem for $\varphi^{(2,1)}$ this way in order to emphasize the similarity with the $O(\varepsilon)$ problem.

Thus we immediately conclude that the general solution for $\varphi^{(2,1)}$ can be written in the form

$$\varphi^{(2,1)} = \left\{\gamma_{21}\Phi(\chi) + \frac{2}{5}\left[F_2(\chi) + \frac{254}{25}F_3(\chi)\right]\right\}A\exp(3i\theta) + \text{c.c.}, \tag{3.49}$$

where the constant γ_{21} is chosen so that the solution matches with the $O(\varepsilon^2\ln\varepsilon)$ term in (3.22) for large $|\chi|$.

It follows that

$$\begin{aligned}\varphi^{(2,1)}(\theta,\chi,X,T,\tau) \simeq A\exp(3i\theta)\Bigg[&-\frac{14\chi}{15} + \left(\frac{58}{25} + \frac{2\gamma_{21}}{3}\right)\frac{1}{\chi} + \cdots\\ &+ \left(\frac{48}{25\chi} + \cdots\right)\ln|\chi|\Bigg] + \text{c.c.},\end{aligned} \tag{3.50}$$

as $|\chi| \to \infty$. This expression will match with the $O(\varepsilon^2 \ln \varepsilon)$ term in (3.22) if

$$\frac{58}{25} + \frac{2\gamma_{21}}{3} = \frac{2066}{875} - \frac{4i(A_T + A_X)}{15A} = -\frac{914}{2625},$$

which implies

$$\gamma_{21} = -\frac{3502}{875}. \tag{3.51}$$

Thus, the solution for $\varphi^{(2,1)}$ may be written in the form

$$\varphi^{(2,1)} = \left\{ \frac{2}{5} F_2(\chi) + \frac{508}{125} F_3(\chi) - \frac{3502}{875} \Phi(\chi) \right\} A \exp(3i\theta) + \text{c.c.} \tag{3.52}$$

4. Numerical simulation. Equation (2.1) was numerically solved as the system

$$q_t + J(\psi, q) = \frac{1}{R_e} \Delta q, \tag{4.1}$$

$$\Delta \psi = q, \tag{4.2}$$

where $q(x, y, t)$ is the vorticity and R_e is the Reynolds number. In our numerical work, we assume a Reynolds number of $R_e = 3.125 \times 10^8$ to effectively smooth out very high wavenumber features without significantly altering, over the time scales of interest here, the flow evolution.

The numerical procedure we use is a second-order accurate 256×256 finite-difference leap-frog technique, see, e.g., [**19, 22**], in which the Jacobian term is finite differenced using the Arakawa [**1**] scheme. The Arakawa scheme preserves the skew-symmetry, energy and enstrophy conservation properties of the Jacobian. To suppress the development of the computational mode, a Robert filter [**2**] is applied at each time step with a coefficient of 0.005. The stream function was obtained at the end of each time step by inverting (4.2) using a direct solver.

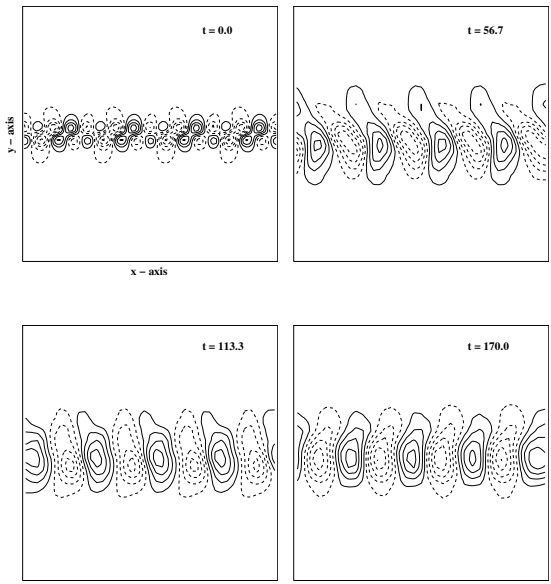

FIGURE 1. Contour plots of the perturbation stream function.

Our simulations are done in a periodic channel domain, denoted as Ω, given by

$$\Omega = \{(x, y) \mid |x| < x_L, |y| < y_L\}, \tag{4.3}$$

in which y_L is chosen so as to have no noticeable effect on the transverse evolution of the perturbation stream function. We assume that the perturbation stream function, in this section denoted as $\phi(x, y, t)$, i.e.,

$$\phi(x, y, t) \equiv \psi(x, y, t) - \varphi_0(y), \tag{4.4}$$

satisfies homogeneous Dirichlet boundary conditions on the transverse boundaries, i.e.,

$$\phi(x, \pm y_L, t) = 0, \tag{4.5}$$

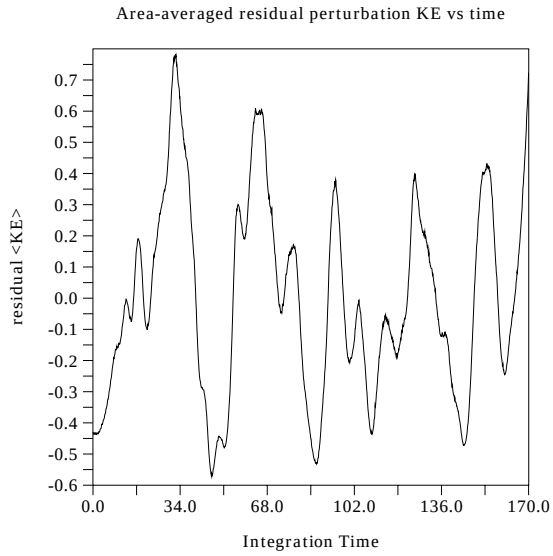

FIGURE 2a.

and we assume that ψ is smoothly periodic along $x = \pm x_L$.

The value of the vorticity on the channel walls was updated using second-order accurate one-sided interior domain differences. We remark that, since we are assuming inviscid boundary conditions, this is an appropriate technique for updating the vorticity on the boundaries.

Since we are using a leap-frog procedure to numerically integrate forward in time, we need initial data not only at $t = 0$ but also at the first time step, say $t = \Delta t$. The initial condition is a linear superposition of the leading order near-singular $k = 3$ mode and the leading order $k = 6$ harmonic, as determined by the weakly nonlinear asymptotic theory and can be written in the form

$$\begin{aligned}\psi(x,y,t) = &-\tanh(y) + \{A\varphi_3(y)\exp(3i[x-(1-\varepsilon)t]) \\ &+ A^2\varphi_6(y)\exp(6i[x-(1-\varepsilon)t]) + \text{c.c.}\},\end{aligned} \tag{4.6}$$

where $\varphi_3(y)$ is the spatially uniformly valid leading order solution to the linear stability problem for the near-singular $k = 3$ mode, i.e., the

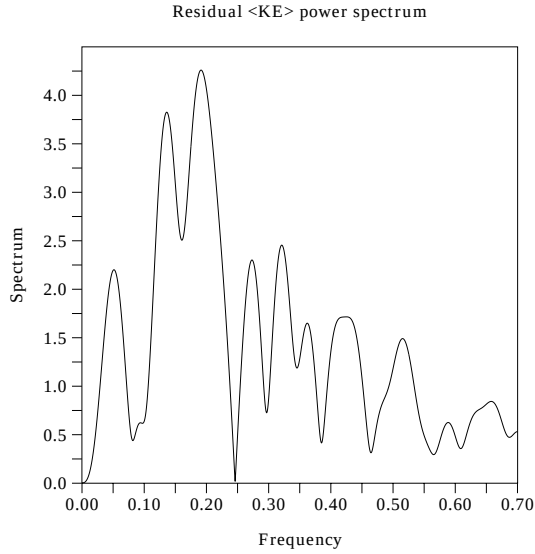

FIGURE 2b.

sum $\varepsilon^3 \times (3.11) + \varepsilon^{5/2} \times (3.31)$ minus the overlap term, and is given by (4.7)

$$\varphi_3(y) = \frac{2\varepsilon^3}{3}\left[\operatorname{sech}^3(y)\coth(y) - \frac{1}{y}\right] + \varepsilon^{\frac{3}{2}}\left[\sqrt{\varepsilon}y + \frac{\varepsilon - y^2}{2}\ln\left(\frac{y+\sqrt{\varepsilon}}{y-\sqrt{\varepsilon}}\right)\right],$$

and where $\varphi_6(y)$, which describes the leading order transverse structure of the $k = 6$ harmonic, is given by

$$\varphi_6(y) = \varepsilon^3\left\{\frac{\varepsilon y}{4(\varepsilon - y^2)} - \sqrt{\varepsilon}\ln\left(\frac{y+\sqrt{\varepsilon}}{y-\sqrt{\varepsilon}}\right) + \frac{y}{4}\ln^2\left(\frac{y+\sqrt{\varepsilon}}{y-\sqrt{\varepsilon}}\right)\right\}, \tag{4.8}$$

where we have written the initial condition in terms of the variable y.

We assumed $A = \delta = 1.0$ and $\varepsilon = 0.05$. Thus $c = 0.95$ and the critical levels are located at $\pm\sqrt{\varepsilon} \simeq 0.22$. We choose $x_L = y_L = 4\pi/3$. With our grid spacing we had about 13 grid points in between the critical levels, i.e., in the region $|y| < \sqrt{\varepsilon}$, at least initially, for each value of x.

In Figure 1 we show four contour plots of the perturbation stream function for $t = 0.0$, 56.7, 113.3 and 170.0, respectively. The solid and dashed lines correspond to positive and negative stream function values, respectively. The perturbation stream function remains rather stable over the integration although there appears to be some dilation in the individual high and lows.

As a measure of the long time variability, we computed the area-averaged perturbation kinetic energy normalized by its initial value, denoted as $\langle KE \rangle$, given by

$$\langle KE \rangle(t) = \frac{\iint_\Omega \nabla\phi \cdot \nabla\phi \, dx \, dy}{\iint_\Omega \nabla\phi \cdot \nabla\phi|_{t=0} \, dx \, dy}. \tag{4.9}$$

Since the domain is a periodic channel and the perturbation stream function was set to zero on the channel walls, the integrals in the $\langle KE \rangle$ effectively integrate out the "fast phase" contributions and

$$\langle KE \rangle(t) \approx |A|^2(t), \tag{4.10}$$

to leading order (recall $A(0) = 1.0$).

In order to show the variability in the $\langle KE \rangle$ we found it effective to de-trend by subtracting out the slight linear trend from the "raw" $\langle KE \rangle$ giving what we call the "residual" $\langle KE \rangle$. In Figure 2a we show the residual $\langle KE \rangle$ versus time. One can see that there is a dominant contribution with a period of about 32 time units. This is a longer time scale than the period associated with the underlying fast phase oscillations which is about $2\pi/(kc) \approx 2.2$ time units.

In Figure 2b we show the power spectrum associated with the residual $\langle KE \rangle$. The highest peak is located at a frequency of about 0.19 which corresponds to a period of about 32 time units. This energy peak appears to be somewhat broad with a secondary peak at about frequency 0.13. Nevertheless Figure 2 suggests a periodic structure to the perturbation stream function amplitude on a time scale longer than the underlying fast phase oscillations.

We are also interested in examining the evolution of the spectral structure to the perturbation stream function. To examine the spectral structure, we computed the one-dimensional wave number power

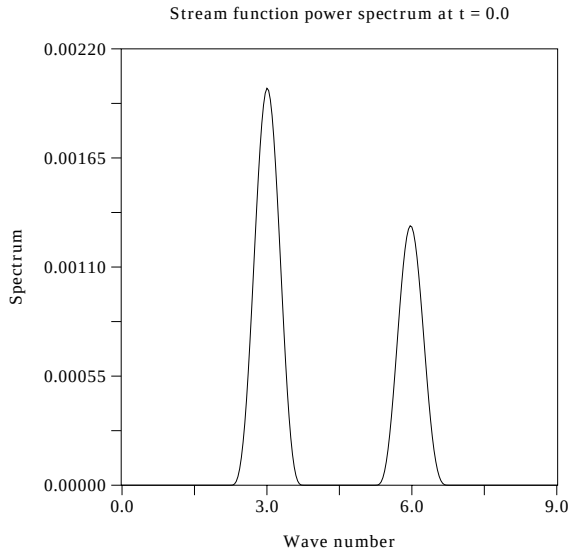

FIGURE 3a.

spectrum of the perturbation stream function with respect to x. This, by itself, would give a function which depends on the x-direction wave number, given by k, and y and t. Because there was little variation as a function of y, it was convenient to average the resulting spectra over y to come up with a power spectrum for the perturbation stream function which is a function of the x-direction wave number and time alone. We denote the resulting spectrum as $\mathcal{S}(k,t)$, and it is given by, see [**12**],

$$\mathcal{S}(k,t) = \frac{1}{2\pi L^2} \int_{-y_L}^{y_L} dy \left| \int_{-x_L}^{x_L} \phi(x,y,t) \exp(-ikx)\, dx \right|^2, \tag{4.11}$$

where $L = 2x_L = 2y_L$ and where the integrals were evaluated using the trapezoidal rule.

In Figure 3a we present a line plot of $\mathcal{S}(k,0)$ versus k. The higher peak located at $k = 3$ corresponds to the contribution from the term

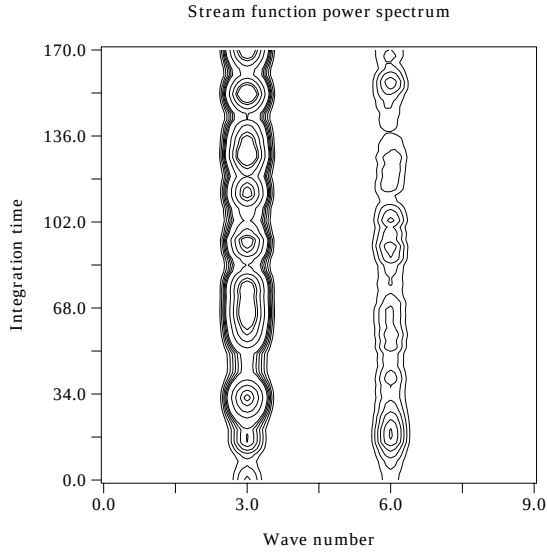

FIGURE 3b.

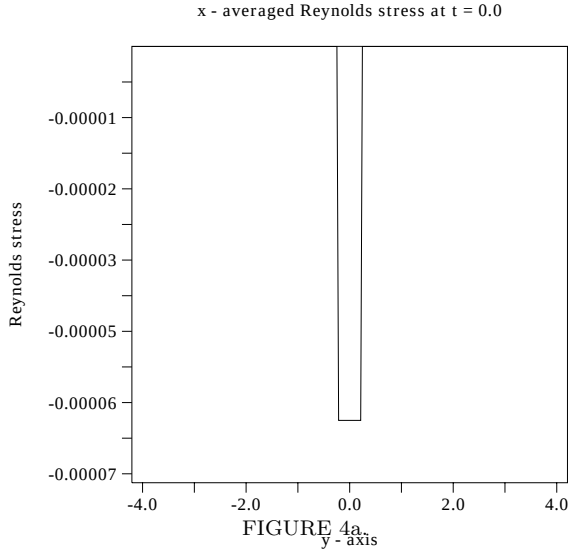

FIGURE 4a.

proportional to A in (4.6), i.e., the uniformly valid leading order solution as obtained from the Rayleigh stability equation for ε small. The lower peak located at $k = 6$ corresponds to the contribution associated with the leading order higher harmonic in the initial condition. The relative size of the two peaks is a result of the asymptotic solution and was not adjusted in an ad hoc manner.

In Figure 3b we present a contour plot of $\mathcal{S}(k,t)$ over the integration time $t \in [0, 170.0]$. We see that, as time unfolds, there is long time variability in the amplitude in the stream function power spectrum. However, Figure 3b also suggests that there is little "leakage" into other wave numbers. There did not seem to be a clearly discernible phase lag between the variability in the $k = 3$ and $k = 6$ contributions.

Up until now, the properties we have seen in the simulation described here are not much different than those seen in the monochromatic simulations described by Swaters [**23**], but this changes when we examine the transverse Reynolds stress in our simulations. As a numerical surrogate for the Reynolds stress, averaged over one wavelength, we computed the Reynolds stress averaged over the computational x domain, which we call τ, defined by

$$\tau(y,t) = -\frac{1}{L}\int_{-x_L}^{x_L} u(x,y,t)v(x,y,t)\,dx, \tag{4.12}$$

where $u(x,y,t)$ and $v(x,y,t)$ were obtained using second-order accurate finite differences from the perturbation stream function $\phi(x,y,t)$.

In Figure 4a we show $\tau(y,0)$ versus y. We see that the numerically computed Reynolds stress is zero in the regions $|y| > \sqrt{\varepsilon}$ and that it is essentially constant in the region $|y| < \sqrt{\varepsilon}$.

In Figure 4b we show a contour plot of $\tau(y,t)$ over the integration time $t \in [0, 170.0]$. The solid and dashed contours correspond to positive and negative values of τ, respectively. As time develops there seems to be a broadening of the region over which the Reynolds stress is nonzero. This broadening continues until about $t = 25$, after which a steady state seems to develop. There is no apparent consistency to the variability.

This is quite different from the monochromatic simulation described by Swaters [**23**, see Figure 7]. In that simulation the Reynolds stress

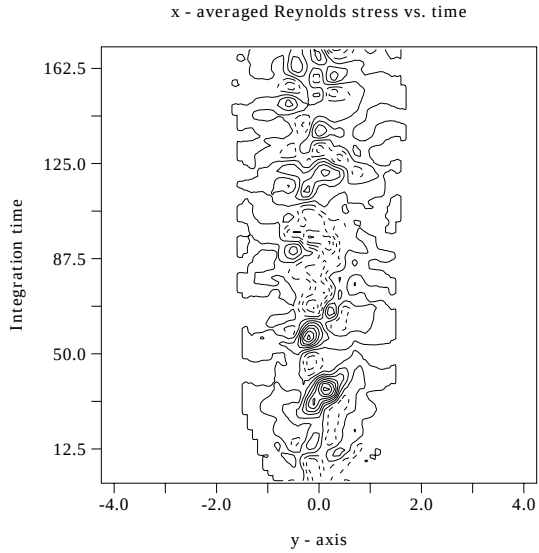

FIGURE 4b.

remained confined to the region $|y| < \sqrt{\varepsilon}$, consistent with monochromatic neutral mode instability theory, and there was a clearly defined slow time oscillation in the x-averaged Reynolds stress which was associated with an oscillatory energy flux from one critical level to other and back again and so on. This pattern apparently does not appear in Figure 4b although one might suggest that in the region $(-\sqrt{\varepsilon} < y < \sqrt{\varepsilon}) \cup (0 < t < 170.0)$ there is some evidence that some sort of periodic behavior can be seen.

5. Conclusions. We have reported on some preliminary investigations into the nonlinear development of near-singular modes of the Bickley jet. By "near-singular" we mean neutral modes which possess a phase velocity "close" to the maximum jet velocity. The critical levels for such a perturbation are located "near" the nose of the jet. Our principal objective has been to "seed" numerical simulations with an initial condition as determined from weakly-nonlinear asymptotic analysis which includes both the leading order mode and the first higher harmonic.

Our numerical simulations possess a distinct long time scale oscillation in the area-averaged perturbation kinetic energy. A long time scale

oscillation in the y-averaged x-wave number power spectrum can also be clearly seen. These oscillations suggest a stable quasi-periodic behavior of the modal amplitudes. No side-band instability was observed in the numerical simulation.

Unlike previous numerical simulations initialized with a monochromatic near-singular mode, the simulation described here does not seem to possess a clear periodic structure in the transverse Reynolds stress as a function of time.

It remains a challenging problem to construct a complete asymptotic wave-packet theory for a weakly nonlinear near-singular mode of the Bickley jet. It is to be hoped that such a theory would produce model equations which predict the quasi-periodic behavior our simulations suggest.

Acknowledgments. Preparation of this paper was supported in part by a research grant awarded by the Natural Sciences and Engineering Research Council of Canada.

ENDNOTES

1. The author thanks A.M.J. Davis for help in determining $F_1(\chi)$ and $F_2(\chi)$.

REFERENCES

1. A. Arakawa, *Computational design for long term numerical integration of the equations of fluid motion: Two-dimensional incompressible flow*, Part I. J. Comput. Phys. **1** (1966), 119–143.

2. R.A. Asselin, *Frequency filter for time integrations*, Mon. Wea. Rev. **100** (1972), 487–490.

3. D.J. Benney, *Nonlinear wave packets on flows with critical layers*, Stud. Appl. Math. **69** (1983), 177–200.

4. D.J. Benney and R.F. Bergeron, Jr., *A new class of nonlinear waves in parallel flows*, Stud. Appl. Math. **48** (1969), 181–204.

5. D.J. Benney and S.A. Maslowe, *The evolution in space and time of nonlinear waves in parallel shear flows*, Stud. Appl. Math. **54** (1975), 181–205.

6. W.G. Bickley, *The plane jet*, Phil. Mag. **23** (1937), 727–731.

7. G. Brunet and P.H. Haynes, *The nonlinear evolution of disturbances to a parabolic jet*, J. Atmos. Sci. **52** (1995), 464–477.

8. B. Brunet and T. Warn, *Rossby wave critical layers on a jet*, J. Atmos. Sci. **47**, 1173–1178.

9. P.G. Drazin and W.H. Reid, *Hydrodynamic stability*, Cambridge University Press, 1981.

10. R. Haberman, *Critical layers in parallel flows*, Stud. Appl. Math. **51** (1972), 139–161.

11. L.N. Howard and P.G. Drazin, *On the instability of parallel shear flow of inviscid fluid in a rotating system with variable Coriolis parameter*, J. Math. Phys. **43** (1964), 83–99.

12. G.M. Jenkins and D.G. Watts, *Spectral analysis and its applications*, Holden-Day, 1968.

13. C.C. Lin, *On the stability of two-dimensional parallel flows*, Quart. Appl. Math. **3** (1945), 117–142.

14. ———, *The theory of hydrodynamic stability*, Cambridge University Press, 1955.

15. F.B. Lipps, *The barotropic stability of the mean winds in the atmosphere*, J. Fluid Mech. **12** (1962), 397–407.

16. S.A. Maslowe, *Barotropic instability of the Bickley jet*, J. Fluid Mech. **229** (1991), 417–426.

17. ———, *Evolution equations for finite amplitude wave packets in parallel shear flows*, Europ. J. Mech. Fluids **10** Suppl. (1991), 289–293.

18. G.E. Mattingly and W.O. Criminale, *The stability of an incompressible two-dimensional wake*, J. Fluid Mech. **51** (1972), 233–272.

19. J.C. McWiliams, G.R. Flierl, V.D. Larichev and G.R. Reznik, *Numerical studies of barotropic modons*, Dynam. Atmos. Oceans **5** (1981), 219–238.

20. P. Savic, *On acoustically effective vortex motion in gaseous jets*, Philos. Mag. **32** (1941), 245–252.

21. M. Stern, *The stability of thermocline jets*, Tellus **13** (1961), 503–508.

22. G.E. Swaters, *A perturbation theory for the solitary drift-vortex solutions of the Hasegawa-Mima equation*, J. Plasma Phys. **41** (1989), 523–539.

23. ———, *On the evolution of near-singular modes of the Bickley jet*, Phys. Fluids **11** (1999), 2546–2555.

24. W. Tollmien, *Ein allgemeines Kriterium der Instabilität laminarer Geschwindigkeitsverteilungen*, Nachr. Wiss. Fachgruppe, Göttingen, Math-phys. Kl. **1** (1935), 79–114. Translated as *General instability criterion of laminar velocity distributions*, Tech. Memor. Nat. Adv. Comm. Aero., Wash. No. **792** (1936).

25. T. Warn and H. Warn, *The evolution of a nonlinear critical layer*, Stud. Appl. Math. **59** (1978), 37–71.

Applied Mathematics Institute, Department of Mathematical Sciences, University of Alberta, Edmonton, Alberta, T6G 2G1, Canada
E-mail address: gordon.swaters@ualberta.ca